Available online at www.sciencedirect.com
SCIENCE DIRECT
Tetrahedron
Tetrahedron 62 (2006) 4285–4293

Synthesis and characterization of porphyrin–ferrocene–fullerene triads

Yongjun Li,[a] Zhenhai Gan,[b] Ning Wang,[a] Xiaorong He,[a] Yuliang Li,[a,*] Shu Wang,[a] Huibiao Liu,[a] Yasuyuki Araki,[b] Osamu Ito[b,*] and Daoben Zhu[a,*]

[a]*CAS Key Laboratory of Organic Solids, Institute of Chemistry, Chinese Academy of Sciences, Graduate School of Chinese Academy of Sciences, Chinese Academy of Sciences, Beijing 100080, People's Republic of China*
[b]*Institute of Multidisciplinary Research for Advanced Materials, Tohoku University, Katahira, Aoba-ku, Sendai, 980-8577 Japan*

Received 31 December 2005; revised 24 February 2006; accepted 27 February 2006

Abstract—Novel porphyrin–fullerene systems linked by ferrocene and related model compounds were successfully synthesized and characterized. Conformationally flexible 1,1′-disubstituted ferrocene functioned as effective modulator of the conformation between porphyrin and fullerene, as ^{1}H NMR spectra indicated, the porphyrin and C_{60} moieties in the triads showed *gauche* type conformation. The electrochemical and photophysical studies showed that there were considerable interactions between porphyrin and fullerene in the ground state due to intramolecular π-stacking of the these two chromophores, assisted by the ferrocence linker. Fluorescence lifetime measurements indicated there might be two different quenching processes occurring simultaneously (intersystem crossing and electron transfer).

1. Introduction

Studies on systems bearing photoactive and electroactive entities have drawn considerable attention as building blocks to construct artificial light energy harvesting systems and also to develop molecular electronic devices.[1–5] In particular, the combination of porphyrins and fullerene has been employed to attain long-lived charge-separated states in high quantum yields.[6–11] Fullerenes are suitable for efficient electron transfer because of their three-dimensional structure, low reduction potentials, and strong electronic acceptor properties.[12–15] Porphyrins contain an extensively conjugated two-dimensional π system, which is also suitable for efficient electron transfer because the uptake or release of electrons results in minimal structural change upon electron transfer.[16] Rates of electron transfer reactions in donor–acceptor (D–A) systems can be well predicted in light of the Marcus theory of electron transfer,[17,18] once the fundamental electron transfer properties of D and A moieties such as the one-electron redox potentials and the reorganization energies of electron transfer are determined. In other words, the distance between the two groups, their relative spatial orientation, and the nature of the pathway linking the two components can act as conduit for the energy or electron transfer.[2,3,14,19] In order to understand the nature of the dialogue between the C_{60} and the porphyrin chromophores, the topology of the two moieties in dyads has been systematically varied and a wide range of covalent and non-covalent assemblies have been reported.[6,10,14,20,21] Ferrocene derivatives are electron donors with considerably low oxidation potentials, which have been employed for the multi-step charge-separation systems of the triad and tetrad molecules.[22,23] Furthermore, porphyrin–ferrocene conjugates have great potential in many areas such as chemical sensors, porphyrin-assisted electron transfer, solar energy conversion and molecular devices.[24–28] An especially interesting issue is the conformation of the 1,1′-disubstituted ferrocene as for these two arms disposed in the same, *gauche*, or opposite directions. The porphyrin (P) and C_{60} moieties in dyads linked by conformationally flexible 1,1′-disubstituted ferrocene may be in close proximity due to π-stacking interactions. Such conformations can facilitate through-space dialogue between the donor and acceptor, as demonstrated by efficient and rapid quenching of porphyrin fluorescence and generation of C_{60} excited states (by energy transfer) or $P_{Zn}^{\cdot+}$–$C_{60}^{\cdot-}$ CS states (by electron transfer).[29] To get more insight into the influence of molecular topology on photoinduced electron transfer, we designed and synthesized P–Fc–C_{60} triads in which the separation and orientation of the π-systems would be controlled by the 1,1′-disubstituted ferrocene (their chemical structures as shown in Chart 1).

Keywords: Porphyrin; Ferrocene; Fullerene; Conformation.
* Corresponding authors. Tel.: 086 10 6258 8934; fax 086 10 8261 6576 (Y.L.); fax: 081 22 217 5608 (O.I.); e-mail addresses: ylli@iccas.ac.cn; ito@tagen.tohoku.ac.jp

0040–4020/$ - see front matter © 2006 Elsevier Ltd. All rights reserved.
doi:10.1016/j.tet.2006.02.076

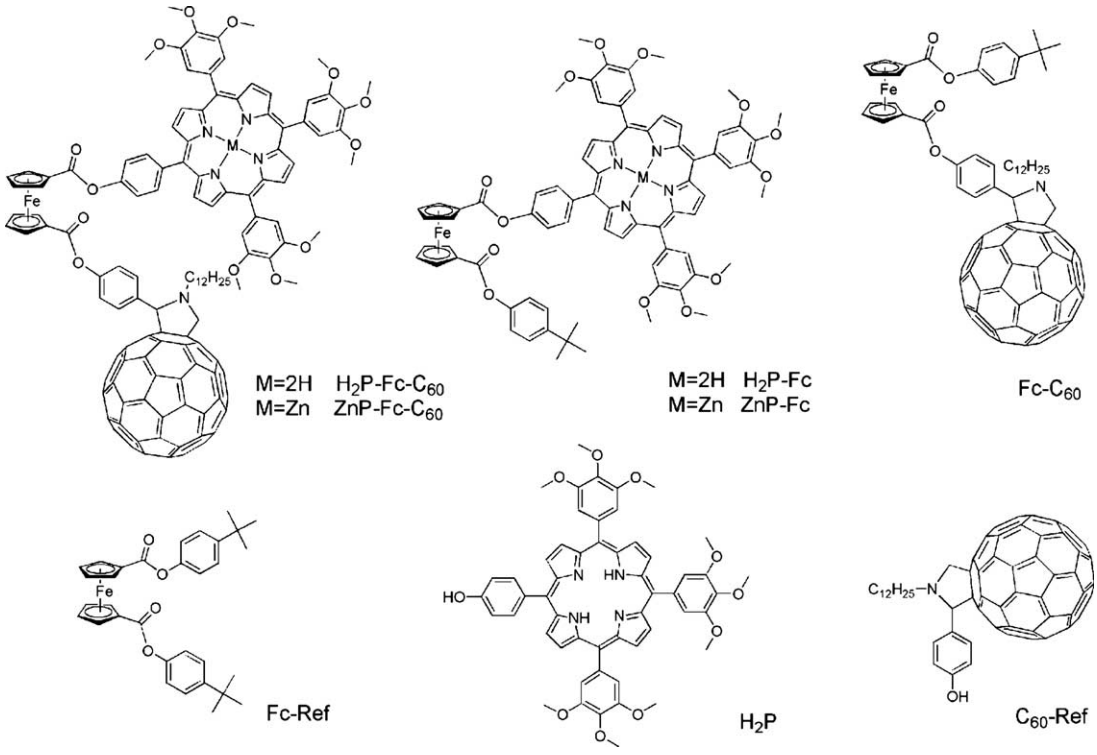

Chart 1.

2. Results and discussion

2.1. Synthesis and characterization

The general strategy employed for the synthesis of **H_2P–Fc–C_{60}** was summarized in Scheme 1. The preparation of **H_2P–Fc–C_{60}** was achieved in a simple 'one-pot' stepwise procedure.[26] **H_2P–Fc**, **Fc–C_{60}** and **Fc-ref** were prepared by following the similar procedures. Their structures were verified by spectroscopic analyses including ^{1}H NMR and MALDI-TOF mass spectra (see Section 4).

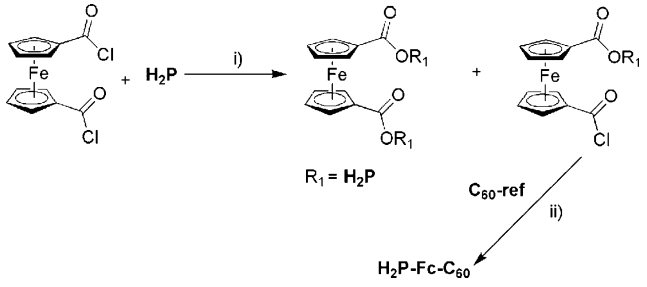

Scheme 1. Synthesis route of **H_2P–Fc–C_{60}**: (i) Et_3N/CH_2Cl_2, rt, N_2, 10 min; (ii) Et_3N/CH_2Cl_2, rt, N_2, 3 h.

2.2. Conformations of porphyrin–ferrocene–C_{60} triad

The distance between the electron donor and acceptor in a D–A system is one of the key factors that control the feasibility and kinetics of electron and energy transfer.[21] This distance is regulated by the conformational properties of the system. The conformation of 1,1′-disubstituted ferrocene imposed a notable impact on the mutual orientation of porphyrin and fullerene (Fig. 1).

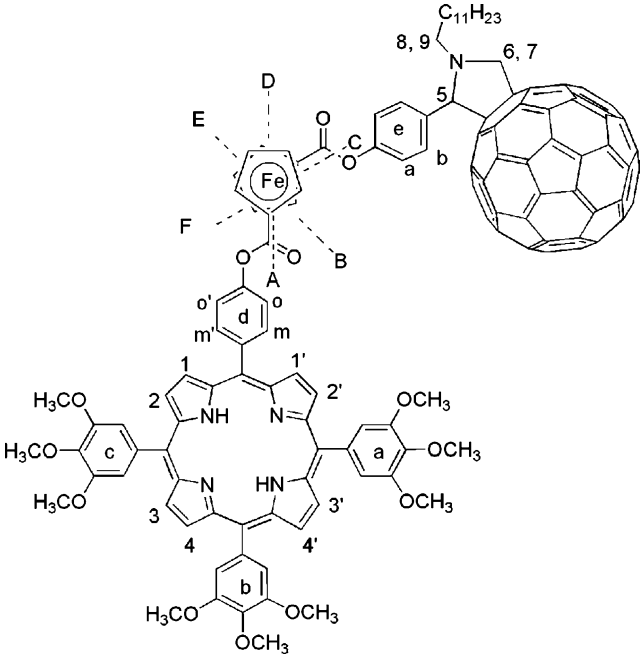

Figure 1. Possible topology of porphyrin–ferrocene–C_{60} hybrids: A-eclipse, B, F-*gauche*, C, D, E-opposite.

There were four conformers of the disubstituted ferrocene as depicted in Figure 1: the 'eclipse' isomer (A), the '*gauche*' isomer (B, F), the 'opposite' isomer (D), and an isomer in which the porphyrin was linked at the ferrocene skeleton at the neighboring position of the 'opposite' isomer (C, E). In particular, the *gauche* type conformation [25] was expected to furnish closer contacts and less overlap with the fullerene than the overlap (eclipse) type conformation due to the steric constraints. In the case of **H_2P–Fc** and **Fc–C_{60}**, there

was no π–π interaction in these molecules, and the steric constraint was little; thus, the ferrocene could freely move. This could be found in the ^{1}H NMR spectra.

In phenyl-substituted pyrrolidinofullerene derivatives, **Fc–C_{60}**, **H_2P–Fc–C_{60}**, **ZnP–Fc–C_{60}**, the NMR signals arising from the protons of the phenyl group attached to the pyrrolidine ring were broadened at room temperature by restricted rotation. [30–33] And we also observed the restricted rotation of ferrocene in the case of **H_2P–Fc–C_{60}**, **ZnP–Fc–C_{60}**. At room temperature, the spectra exhibited the expected features with the characteristic signals arising from ferrocene, two AB quartets for β–H of porphyrin, an AB quartet for phenyl ring **d**, an AB quartet and a singlet for the pyrrolidine protons. As shown in Figure 2, the pyrrole signals (two doublets, 8.90 ppm (J=4.6 Hz) and a singlet, 8.96 ppm) of **H_2P** and **H_2P–Fc** were changed into four doublets in **H_2P–Fc–C_{60}** (9.03, 8.94, 8.81, 8.73 ppm, J=4.6 Hz). The aryl protons of phenyl ring **d** in **H_2P–Fc–C_{60}** were up-shielded from that of **H_2P–Fc** (8.22 ppm) to 7.77 ppm. The aromatic protons of trimethoxyphenyl (**a**, **b** or **b**, **c**) in **H_2P–Fc** (7.48 ppm, s) were split into two single (7.63, 7.35 ppm) in the case of **H_2P–Fc–C_{60}**, which indicated that trimethoxyphenyl **a**, **b**, **c** became non-equivalent. In addition, –OCH_3 protons (4.17 ppm (s, 6H), 3.92 ppm (s, 12H)) in two trimethoxyphenyl were shifted to upfield as compared with that of **H_2P–Fc** (4.19 ppm, 3.98 ppm). The NH signal in porphyrin ring was shifted from −2.79 ppm in **H_2P–Fc** to −3.00 ppm in **H_2P–Fc–C_{60}**.

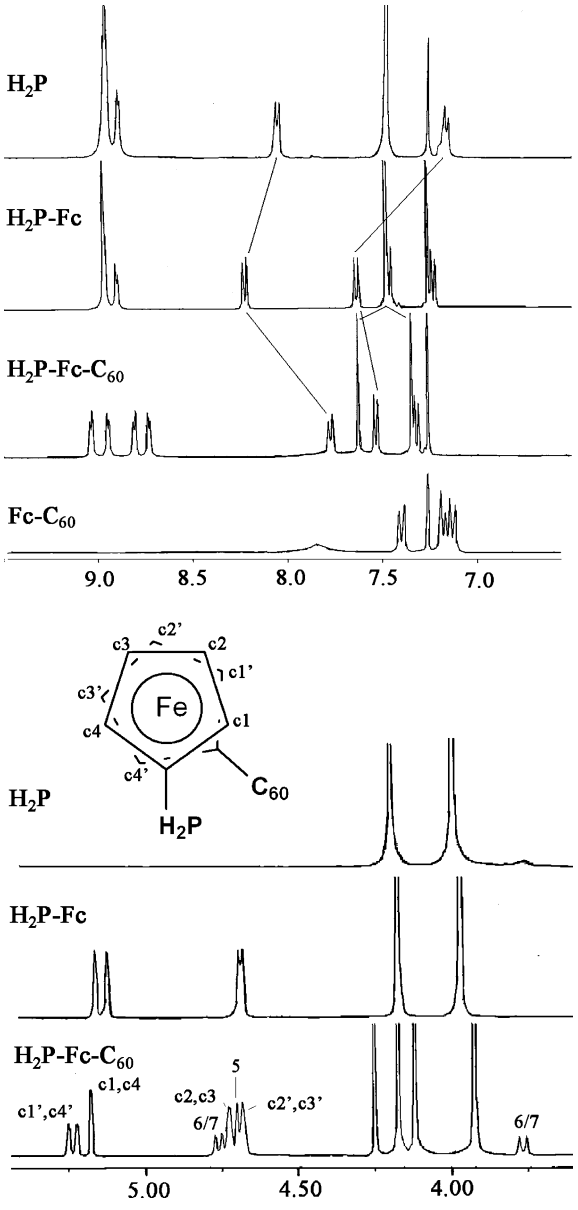

Figure 2. ^{1}H NMR spectra (400 MHz) of **H_2P**, **H_2P–Fc** and **H_2P–Fc–C_{60}** in $CDCl_3$ at room temperature.

The signals corresponding to the protons of the phenyl group directly attached to the pyrrolidine ring were broadened at room temperature. A variable-temperature NMR study showed clear coalescence, and the reversible narrowing of all these peaks revealed a dynamic effect. As typical examples, the ^{1}H NMR spectra of **ZnP–Fc–C_{60}** recorded at different temperatures were shown in Figure 3. At high temperatures, an AB system was seen for the aromatic protons of the phenyl group directly attached to the pyrrolidine ring. And ferrocene rotated faster as attested by the coalescence of some ferrocene protons near 5.25–5.3 ppm. By cooling the solution to −50 °C, the rotation of ferrocene became slow on the NMR timescale, the mutual orientation of porphyrin and fullerene was fixed in a *gauche* type conformation as evidenced by the coalescence of an AB quadruplet for β–H of porphyrin, the broadened signals of *meso*-phenyl group and the methoxy group on it, which was resulted from their position atop the fullerene sphere. At high temperatures, an AA′XX′ system was seen. The exchange between $H_{o/m}$ and $H_{o'/m'}$ was fast on the NMR timescale under these conditions, and both pairs of protons $H_{o/o'}$ and $H_{m/m'}$ appeared equivalent in the ^{1}H NMR spectrum. In contrast, by cooling the solution to −50 °C, the exchange was slow on the NMR timescale, as attested by only one AB quadruplet standing for two protons were observable, and the other two protons facing the fullerene sphere were broadened.

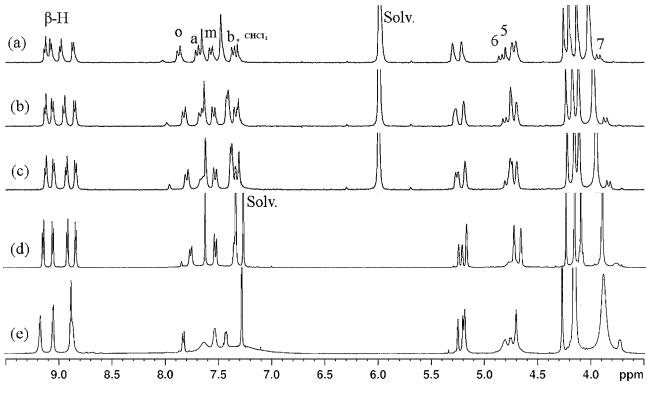

Figure 3. ^{1}H NMR spectra of **ZnP–Fc–C_{60}** recorded in $CDCl_2CDCl_2$ at (a) 107 °C, (b) 67 °C, (c) 47 °C and in $CDCl_3$ at (d) 25 °C, (e) −50 °C.

All these suggested that porphyrin ring was not opposite to C_{60} for steric reasons, but was locked in a *gauche* type conformation.[25] The chemical shifts and the resonance pattern changes of pyrrole protons, the aryl protons of phenyl ring **d**, aromatic protons and –OCH_3 protons of trimethoxyphenyl were all due to the deshielding effect resulted from C_{60} π-electrons, and evidence for these effects

could also be found from UV/vis spectra and electrochemical data for **H_2P–Fc–C_{60}** as shown below.

2.3. Cyclic voltammetric studies

Determination of the redox potentials in the donor–acceptor system is important to prove the existence of charge-transfer interactions between the donor and acceptor in the ground state, and also to evaluate the energetic of electron transfer reactions. The cyclic voltammograms of **H_2P–Fc–C_{60}** and **ZnP–Fc–C_{60}** were shown in Figure 4, and the half-wave potentials ($E_{1/2}$) of them together with those of **H_2P–Fc**, **ZnP–Fc**, **Fc–C_{60}**, **Fc-ref**, and **C_{60}-ref** were summarized in Table 1.

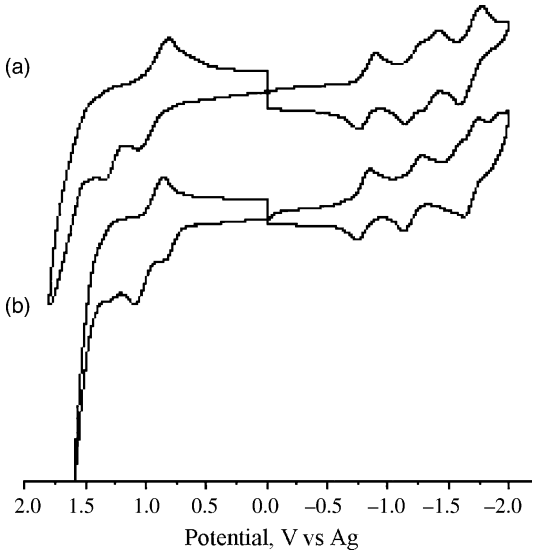

Figure 4. Cyclic voltammograms of (a) **H_2P–Fc–C_{60}** and (b) **ZnP–Fc–C_{60}** in the presence of 0.05 M (n-$C_4H_9)_4PF_6$ in *o*-dichlorobenzene.

The cyclic voltammogram of **H_2P–Fc–C_{60}** showed two reversible reductions with half-wave potentials ($E_{1/2}$) at −0.87 and −1.24 V (vs Ag/Ag^+) based on the fullerene core, one reversible reduction ($E_{1/2}=-1.40$ V) based on porphyrin, and one overlapping reduction ($E_{1/2}=-1.72$ V) corresponding to the fullerene and porphyrin, respectively. The cyclic voltammogram of **ZnP–Fc–C_{60}** showed three reversible reductions at −0.79, −1.20, −1.68 V for the fullerene core, and two reversible reductions at −1.58 and −1.85 V for the porphyrin. The half-wave potentials for the reductions of compounds **H_2P–Fc–C_{60}** and **ZnP–Fc–C_{60}** corresponding to the fullerene moieties were more negative than those of the reference compound **C_{60}-ref** by 80–160 mV, but compared with those of **Fc–C_{60}**, E (**H_2P–Fc–C_{60}** (−0.87 V))$<E$ (**Fc–C_{60}** (−0.83 V))$<E$ (**ZnP–Fc–C_{60}** (−0.79 V)). In **H_2P–Fc–C_{60}**, the one-electron reductions at porphyrin macrocyclic ring occured at more negative potentials as compared to the value of **H_2P–Fc**: E (**H_2P–Fc–C_{60}** (anion radical)) (−1.40 V)$<E$ (**H_2P–Fc**) (−1.34 V). In the case of **ZnP–Fc–C_{60}**, the reductions of porphyrin occured at more positive potentials as compared to the value of **ZnP–Fc**: E (**ZnP–Fc**) (−1.60 V)$<E$ (**ZnP–Fc–C_{60}** (anion radical)) (−1.52 V). That is, the fullerene and porphyrin reduction potentials were anodically shifted in the systems containing the zinc porphyrin, whereas the reverse was observed in the triad with the free-base porphyrin. This could be accounted by another placement of the porphyrin with respect to the fullerene and therefore a different conformation of the molecules, because zinc porphyrin has stronger electron donation ability, it may take a conformation closer to fullerene.

The one-electron oxidation of **H_2P–Fc** and **H_2P–Fc–C_{60}** occurred at the porphyrin macrocyclic ring at 0.94 and 0.95 V, respectively. The one-electron oxidation of ferrocene was overlapped with the oxidation of porphyrin. The first one-electron oxidation potentials of **ZnP–Fc** and **ZnP–Fc–C_{60}** were the same ($E_p=0.84$ V). The second one-electron oxidation potentials ascribed to ferrocene shifted to a more negative value than that of the model compound **Fc-ref** by ∼100 mV for **ZnP–Fc** and ∼40 mV for **ZnP–Fc–C_{60}**. Generally, the zinc porphyrin compounds ($E_p=0.84$ V for **ZnP–Fc–C_{60}** and **ZnP–Fc**, respectively) were considerably easier to oxidize than the corresponding zinc-free porphyrin compounds ($E_{1/2}=0.95$ V for **H_2P–Fc–C_{60}** and $E_{1/2}=0.94$ V for **H_2P–Fc**). Thus, in each case, the first one-electron reduction occurred at the C_{60} moiety, the first one-electron oxidation occurred at the porphyrin macrocyclic ring in the case of **ZnP–Fc–C_{60}**, while in the case of **H_2P–Fc–C_{60}**, it occurred at the porphyrin or ferrocene ring, and there existed interactions between porphyrin and fullerene moiety in the ground state. The **ZnP** and **H_2P** moiety seemed to be electron donating to C_{60}.

2.4. Steady-state absorption spectra

The absorption spectra of **H_2P–Fc–C_{60}**, **H_2P–Fc**, **Fc–C_{60}** and **Fc-ref** in CH_2Cl_2 were shown in Figure 5. The absorption and fluorescence data of **H_2P–Fc–C_{60}**, **H_2P–Fc**, and their zinc complexes were summarized in Table 2. In **H_2P–Fc** and **C_{60}-Fc**, the absorption spectra of the dyads were virtual superposition of the two independent chromophores: the porphyrin component showed a very strong absorption at

Table 1. Half-wave potentials (V vs Ag wire) of triads, dyads and reference compounds in dichlorobenzene containing 0.05 M (n-$C_4H_9)_4PF_6$

	Oxidation			Reduction				
	Porphyrin		Ferrocene	Porphyrin		Fullerene		
	$E_{1/2}(1)$	$E_{1/2}(2)$	$E_{1/2}$	$E_{1/2}(1)$	$E_{1/2}(2)$	$E_{1/2}(1)$	$E_{1/2}(2)$	$E_{1/2}(3)$
Fc-ref			1.01					
C_{60}-ref						−0.71	−1.09	−1.67
Fc–C_{60}			1.00			−0.83	−1.22	−1.81
H_2P–Fc	0.94	1.33[a]	0.94	−1.34	−1.61			
H_2P–Fc–C_{60}	0.95	1.32[a]	0.95	−1.40	−1.72	−0.87	−1.24	−1.72
ZnP–Fc	0.84[a]		0.91	−1.60	−1.77			
ZnP–Fc–C_{60}	0.84[a]	1.30[a]	0.97	−1.52	−1.85	−0.79	−1.20	−1.68

[a] Peak potential.

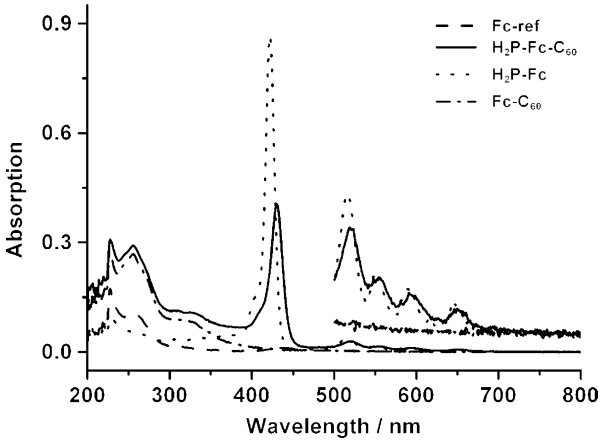

Figure 5. UV/vis spectra of 2 μM of **H_2P–Fc–C_{60}**, **H_2P–Fc**, **Fc–C_{60}**, and **Fc-ref** in CH_2Cl_2 at room temperature, above 500 nm a multiplying factor of 10 is used.

422 nm (Soret band) and four weak absorption at 516, 552, 592 and 646 nm (Q-band), the fullerene showed a strong π–π* band at 330 nm accompanied with weak long-wavelength bands tailing to 700 nm, and the ferrocene had an electronic transition at 444 nm, but its intensity was very weak. Evidently there were no detectable interactions between the chromophores in the ground state. In contrary, a considerable ground-state interaction of the porphyrin and fullerene moieties was seen in the absorption spectrum of **H_2P–Fc–C_{60}** and **ZnP–Fc–C_{60}** in CH_2Cl_2 and less polar solvent as toluene. The close proximity of the porphyrin and fullerene π-systems gave rise to through-space[34–37] and through-bond interaction, which may be detected in the shifts of some absorption bands. As usual, one could observe an absorption band at about 432 nm, a characteristic of the [6, 6] monoadduct of C_{60} in the UV/vis absorption spectra of C_{60} derivatives. In this case, the Soret band at 422 nm of **H_2P** was shifted to 430 nm due to the withdrawing electron effect of C_{60} moiety, the absorption band of the [6, 6] monoadduct of C_{60} was overlapped with that of porphyrin moiety. The absorption maxim of the free-base porphyrin entity in **H_2P–Fc–C_{60}** showed a 8 nm red shift compared to that of the **H_2P–Fc**, 9 nm red-shift was also observed in the case of **ZnP–Fc–C_{60}**, and a strong intensity decrease was seen in **H_2P–Fc–C_{60}**, **ZnP–Fc–C_{60}** when compared to the corresponding absorptions in **H_2P–Fc** and **ZnP–Fc**. Concentration dependence studies (2–20 μM) revealed no changes in the absorption maximal band, suggesting that the interactions were mainly intramolecular in nature.[38] Effectively, red-shifts in the Soret band were observed for covalent C_{60}–porphyrin conjugates due to intramolecular π-stacking of the two chromophores.[39,40]

2.5. Steady-state fluorescence spectra

Fluorescence spectra were taken in both CH_2Cl_2 and toluene with excitation at 420 nm, which excited both porphyrin and C_{60} moieties. The emission spectra of **H_2P–Fc–C_{60}** and **H_2P–Fc** revealed two emission bands located at 652 and 718 nm, respectively. The intensity of these bands of **H_2P–Fc–C_{60}** was significantly quenched as compared to **H_2P–Fc** owing to the presence of the appended C_{60}. A similar phenomenon was observed in the case of **ZnP–Fc–C_{60}** and **ZnP–Fc** (600 and 646 nm). The fluorescence quantum yields (Φ) of these compounds were calculated by the steady-state comparative method using tetraphenylporphyrin (TPP) as a reference (Φ_F=0.11) (Table 2).[41] As can be seen in Figure 6, the fluorescence peak of C_{60} expected to appear at 725 nm may

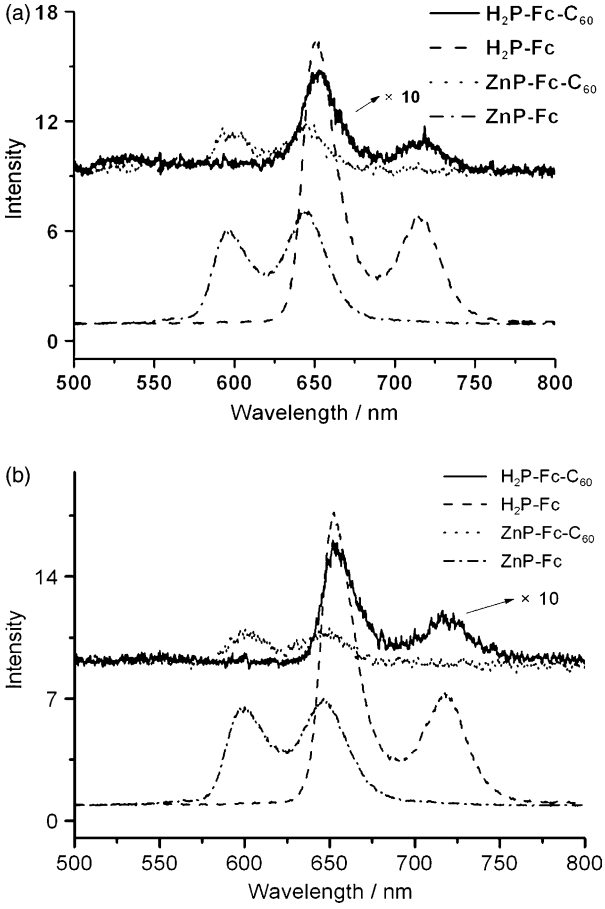

Figure 6. Steady-state fluorescence spectrum of **H_2P–Fc–C_{60}**, **H_2P–Fc**, **ZnP–Fc–C_{60}**, and **ZnP–Fc** (2 μM) in CH_2Cl_2 (a) and toluene (b) at room temperature.

Table 2. Spectroscopic data of the **H_2P–Fc–C_{60}** triads and related compounds

Compound	Solvent	Absorption λ (nm)	Emission for P λ (nm)[a]	Φ ($\times 10^{-3}$) for P[a]
H_2P–Fc–C_{60}	CH_2Cl_2	430, 521, 556, 596, 652	652, 715	7.4
	Toluene	431, 520, 555, 596, 652	653, 718	
ZnP–Fc–C_{60}	CH_2Cl_2	431, 552, 592	596, 644	6.3
	Toluene	433, 553, 593	599, 647	
H_2P–Fc	CH_2Cl_2	422, 516, 552, 592, 646	652, 716	81.9
	Toluene	423, 516, 552, 592, 649	652, 717	
ZnP–Fc	CH_2Cl_2	422, 548, 588	596, 644	44.3
	Toluene	426, 550, 592	599, 646	

[a] λ_{ex}=420 nm.

be hidden in the fluorescence bands of the H_2P moieties, while in the case of **ZnP–Fc–C_{60}**, the fluorescence of the C_{60} moiety was not observed, which suggested that energy transfer from the excited singlet state of the ZnP moiety to the C_{60} moiety may not have taken place, and there was no clear evidence for the existence of the singlet–singlet energy transfer from the porphyrin to the C_{60} in **H_2P–Fc–C_{60}**. These observations indicated that electron transfer predominantly took place from the excited singlet state of the ZnP moiety to the C_{60} moiety through space in CH_2Cl_2 and toluene or intersystem crossing process from singlet porphyrin to triplet porphyrin by ferrocene that had a low-lying triplet state.

2.6. Fluorescence lifetime measurements

To invest the charge separation process, the fluorescence lifetime measurements were carried out from 650 to 800 nm in toluene. Time profiles of the fluorescence intensities of the **H_2P–Fc**, **ZnP–Fc**, **H_2P–Fc–C_{60}** and **ZnP–Fc–C_{60}** in PhCN (λ_{ex}=410 nm.) were shown in Figure 7. In the case of **H_2P–Fc** and **ZnP–Fc**, the decay obeyed single exponential function giving a single fluorescence lifetime as summarized in Table 3. On the other hand decay of **H_2P–Fc–C_{60}** and **ZnP–Fc–C_{60}** consisted of fast decay component and slow component, from which two lifetimes were evaluated as listed in Table 3. Appreciable increase in the decay rates was observed for **H_2P–Fc–C_{60}** when C_{60} was linked to **H_2P–Fc**, while only slight increase was observed for **ZnP–Fc–C_{60}** when C_{60} was linked to **ZnP–Fc**. Similar results were obtained in benzonitrile (Table 3). From the shorter lifetime compared with tetraphenylporphyrin in polar and nonpolar solvents, it was suggested that there may be electron transfer or energy transfer when porphyrin was linked to ferrocene and ferrocene–fullerene. In the **H_2P–Fc** and **ZnP–Fc** case, there was no radical to be found when the samples were excited by 532 nm laser in our preliminary nanosecond transient measurement. So the short lifetime of fluorescence may be due to the addition of ferrocene moiety to accelerate the intersystem crossing process from singlet porphyrin to triplet porphyrin by ferrocene. On the other hand, there were electron transfer or energy transfer be observed from the excited singlet state of porphyrin to fullerene in the case of **H_2P–Fc–C_{60}** and **ZnP–Fc–C_{60}**. These rate constants could be calculated from the fluorescence lifetimes.

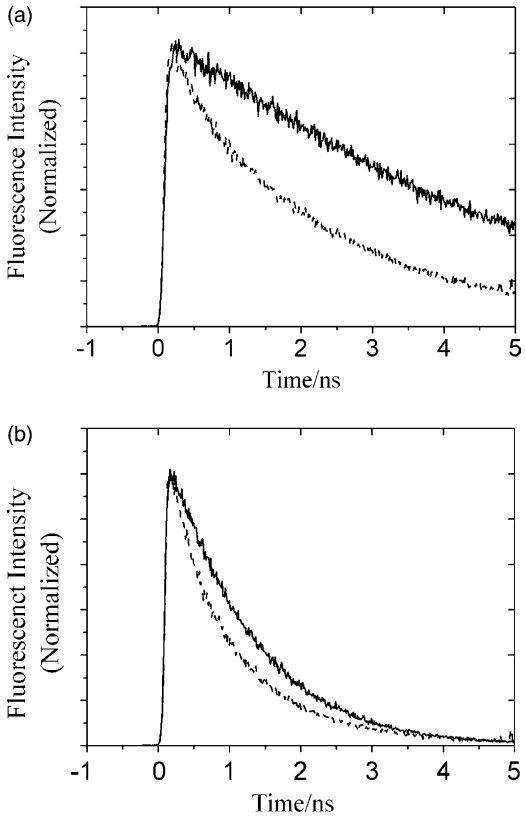

Figure 7. Time profiles of fluorescence lifetime measurement of (a) **H_2P–Fc** (solid line) and **H_2P–Fc–C_{60}** (dotted line, 0.05 mM); (b) **ZnP–Fc** (solid line) and **ZnP–Fc–C_{60}** (dotted line, 0.05 mM) in toluene. λ_{ex}=410 nm.

The rate constants (k_q) and quantum yields (Φ_q) of the fluorescence quenching of ^{1}**H_2P^*** or ^{1}**ZnP***, **H_2P–Fc**, **ZnP–Fc**, **H_2P–Fc–C_{60}** and **ZnP–Fc–C_{60}** in toluene and benzonitrile were evaluated by the following Eqs. 1 and 2, in which the $(\tau_f)_{ref}$ is referred to the fluorescence lifetimes of tetraphenylporphyrins.

$$k_q = (1/\tau_f)_{sample} - (1/\tau_f)_{ref} \quad (1)$$

$$\Phi_q = [(1/\tau_f)_{sample} - (1/\tau_f)_{ref}]/(1/\tau)_{sample} \quad (2)$$

The k_q and Φ_q values were evaluated as listed in Table 3.

The lifetime measurements indicated two components in the fluorescence of the triads, but none of them corresponded to that determined in the porphyrin–ferrocene dyads. There might be two different quenching processes occurring simultaneously (intersystem crossing and electron transfer). From the lifetime data and quenching quantum yields indicated in Table 3, one could observe that intersystem crossing represented an important percentage of the quenching. Besides, the quenching rate of the porphyrin was not sensitive to solvent polarity (Table 3). If electron transfer was the major quenching pathway, the very large

Table 3. Fluorescence lifetime (τ_f), fluorescence quenching rate-constants (k_q), fluorescence quenching quantum-yields (Φ_q) of **H_2P–Fc**, **ZnP–Fc**, **H_2P–Fc–C_{60}** and **ZnP–Fc–C_{60}** in toluene and benzonitrile (PhCN)

Solvent	Sample	τ (ns) (%)	k_q (s^{-1})	Φ_q
Toluene	**H_2P–Fc**	4.66 (100%)	1.4×10^8	0.66
	H_2P–Fc–C_{60}	0.42 (15%), 2.43 (85%)	3.8×10^8	0.84
	ZnP–Fc	1.15 (100%)	5.0×10^8	0.57
	ZnP–Fc–C_{60}	0.57 (52%), 1.35 (48%)	6.9×10^8	0.65
PhCN	**H_2P–Fc**	5.39 (100%)	8.6×10^7	0.47
	H_2P–Fc–C_{60}	0.38 (24%), 4.17 (76%)	2.1×10^8	0.68
	ZnP–Fc	1.21 (100%)	3.5×10^8	0.43
	ZnP–Fc–C_{60}	0.722 (66%), 844 (34%)	4.3×10^8	0.47

difference of the electron transfer driving force when passed from toluene to benzonitrile should alter the kinetics. Furthermore, electron transfer driving force was higher for the **ZnP** system, but surprisingly, it was less quenched than the **H_2P** system.

3. Conclusions

In summary, novel porphyrin–fullerene system linked by ferrocene and related model compounds were synthesized and characterized. The porphyrin (P) and C_{60} moieties in triads linked by conformationally flexible 1,1′-disubstituted ferrocene showed *gauche* type conformation, as indicated by the ^{1}H NMR spectra. The electrochemical and photophysical studies showed that there were considerable interactions between the two chromophores in the ground state and the excited singlet state. Fluorescence lifetime measurements indicated there may be two different quenching processes occurring simultaneously (intersystem crossing and electron transfer). The detailed photophysical study is in progress.

4. Experimental

4.1. General

Reagents were of reagent grade quality, obtained commercially and used without further purification except as noted elsewhere. All solvents were purified using standard procedures. Evaporation and concentration in vacuum were done at water aspirator pressure and compounds were dried at 10^{-2} Torr. FT-IR spectra were recorded as KBr pellets on a Perkin-Elmer system 2000 spectrometer. ^{1}H NMR spectra were measured on Bruker ARX400 or DMX300 spectrometers. Matrix-assisted laser desorption/ionization (MALDI) time-of-flight mass spectra (TOF) were measured on a Bruker Biflex III MALDI-TOF. Steady-state absorption spectra in the UV and the visible regions were measured on a Hitachi U-3010 spectrometer. Steady-state fluorescence spectra were measured on a Hitachi F-4500 spectrometer.

The cyclic voltammetry measurements were performed on a CHI660B electrochemical analyzer in a deaerated *o*-dichlorobenzene solution containing 0.05 M $(C_4H_9)_4PF_6$ as a supporting electrolyte at room temperature (100 mV s^{-1}). The counter electrode was a platinum wire. The measured potentials were recorded with respect to an Ag wire (Ag/Ag^+) reference electrode.

The lifetimes of the fluorescence bands were measured by a single-photon counting method using a second harmonic generation (SHG, 410 nm) of a Ti–sapphire laser (Spectra-Physics, Tsunami 3950-L2S, 1.5 ps fwhm) and a streak-scope (Hamamatsu Photonics, C43334-01) equipped with a polychromator (Action Research, SpectraPro 150) as an excitation source and a detector, respectively. Lifetimes were evaluated with software attached to the equipments.

4.1.1. Synthesis of H_2P–Fc–C_{60}. A solution of 1,1′-bis(chlorocarbonyl) ferrocene[42] (31 mg, 0.1 mmol), 5-(*p*-hydroxyphenyl)-10,15,20-tri (3,4,5-trimethoxyphenyl)-porphyrin[43] (90 mg, 0.1 mmol), and triethylamine (1 ml) in dry CH_2Cl_2 (100 ml) was stirred for 10 min at room temperature under N_2. To the reaction mixture was added **C_{60}-ref**[43] (102 mg, 0.1 mmol), and then the resulting mixture was stirred for another 3 h. The solution was washed with water, dried over anhydrous sodium sulfate. After evaporation, the residue was purified by column chromatography (SiO_2 (160–200 meshes), $CHCl_3/CH_2Cl_2$/EtOAc, 5:5:1) to give **H_2P–Fc–C_{60}** as a dark solid (107 mg, 50%). ^{1}H NMR (400 MHz, $CDCl_3$): 9.03 (d, J=4.6 Hz, 2H), 8.94 (d, J=4.6 Hz, 2H), 8.81 (d, J=4.6 Hz, 2H), 8.73 (d, J=4.6 Hz, 2H), 7.77 (d, J=7.8 Hz, 2H), 7.63 (s, 2H), 7.53 (d, J=7.8 Hz, 2H), 7.35 (s, 4H), 7.32 (d, J=8.6 Hz, 2H), 5.25 (d, J=1.1 Hz, 1H), 5.22 (d, J=1.1 Hz, 1H), 5.17 (d, J=1.6 Hz, 2H), 4.76 (d, J=9.2 Hz, 1H), 4.72 (d, J=1.3 Hz, 2H), 4.70 (s, 1H), 4.65–4.70 (m, 2H), 4.25 (s, 3H), 4.17 (s, 6H), 4.12 (s, 6H), 3.92 (s, 12H), 3.76 (d, J=9.1 Hz, 1H), 3.05–3.20 (m, 1H), 2.34–2.42 (m, 1H), 1.75–1.85 (m, 2H), 1.43–1.24 (m, 18H), 0.87–0.93 (m, 3H), −3.00 (s, 2H). ^{13}C NMR (100 MHz, $CDCl_3$): 169.5, 169.2, 155.6, 153.5, 152.6, 152.4, 151.5, 151.3, 150.7, 150.4, 145.7, 145.2, 144.7, 144.1, 143.5, 143.3, 143.1, 142.9, 141.7, 141.5, 141.3, 141.0, 140.1, 139.5, 139.2, 138.8, 138.4, 137.9, 137.8, 137.7, 137.6, 135.8, 134.9, 131.5, 130.4, 120.4, 120.2, 120.1, 119.2, 112.7, 112.6, 96.1, 81.7, 73.0, 72.7, 72.5, 68.3, 66.5, 61.4, 61.3, 56.6, 56.4, 53.1, 31.9, 29.7, 29.3, 28.4, 27.5, 22.7,14.1. UV/vis (CH_2Cl_2) λ_{max} 430, 521, 556, 596, 652 nm; fluorescence (CH_2Cl_2) λ_{max} 652, 715 nm; FT-IR (KBr, cm^{-1}): 3313, 2924, 2851, 1735, 1579, 1502, 1456, 1407, 1357, 1267, 1235, 1197, 1165, 1126, 1104, 1012, 920.5, 801, 730, 526. MALDI-TOF MS *m/z*: 2161 $[M+H]^+$, 1441 $[M+H]^+-720$, calcd=2161.6 ($C_{145}H_{87}N_5O_{13}Fe$). Anal. Calcd for $C_{145}H_{87}N_5O_{13}Fe$: C, 80.51; H, 4.05; N, 3.24. Found: C, 80.44; H, 4.12; N, 3.27.

4.1.2. H_2P–Fc, C_{60}-ref and Fc-ref were prepared according to the same procedure of H_2P–Fc–C_{60}. H_2P–Fc: ^{1}H NMR (400 MHz, $CDCl_3$): 8.96 (s, 6H), 8.90 (d, J=4.6 Hz, 2H), 8.22 (d, J=8.2 Hz, 2H), 7.63 (d, J=8.2 Hz, 2H), 7.48 (s, 6H), 7.46 (d, J=9.2 Hz, 2H), 7.23 (d, J=8.5 Hz, 2H), 5.23 (s, 2H), 5.19 (s, 2H), 4.72–4.75 (m, 4H), 4.19 (s, 9H), 3.98 (s, 18H), 1.30 (s, 9H), −2.79 (s, 2H). UV/vis (CH_2Cl_2) λ_{max} 422, 516, 552, 592, 646 nm; fluorescence (CH_2Cl_2) λ_{max} 652, 716 nm; FT-IR (KBr, cm^{-1}): 3160, 2937, 1733, 1580, 1502, 1457, 1408, 1358, 1271, 1235, 1202, 1169, 1103, 1011, 922, 802, 729, 520. MALDI-TOF MS *m/z*: 1289 $[M+H]^+$, calcd=1288.4 ($C_{75}H_{68}N_4O_{13}Fe$). Anal. Calcd for $C_{75}H_{68}N_4O_{13}Fe$: C, 69.87; H, 5.32; N, 4.35. Found: C, 69.81; H, 5.38; N, 4.28.

Fc–C_{60}: ^{1}H NMR (300 MHz, $CDCl_3$): 7.97–7.75 (s, br, 2H), 7.42 (d, J=8.3 Hz, 2H), 7.19 (d, J=7.5 Hz, 2H), 7.15 (d, J=8.3 Hz, 2H), 5.12 (m, 1H), 5.06 (d, J=5.3 Hz, 4H), 4.63 (s, 4H), 4.15–4.25 (m, 1H), 3.20–3.35 (m, 1H), 2.50–2.71 (m, 1H), 1.85–2.08 (m, 2H), 1.25–1.47 (m, 27H), 0.81–0.95 (m, 3H). FT-IR (KBr, cm^{-1}): 2954, 2923, 2851, 2796, 1735, 1507, 1457, 1270, 1199, 1168, 1102, 1019, 913, 526. MALDI-TOF MS *m/z*: 1412 $[M+H]^+$, 692 $[M+H]^+-720$, calcd=1411.3 ($C_{102}H_{53}NO_4Fe$). Anal. Calcd for $C_{102}H_{53}NO_4Fe$: C, 86.74; H, 3.78; N, 0.99. Found: C, 86.83; H, 3.77; N, 1.02.

Fc-ref:[25] ^{1}H NMR (300 MHz, $CDCl_3$): 7.38 (d, J=8.3 Hz, 4H), 7.11 (d, J=8.3 Hz, 4H), 5.05 (s, 4H), 4.59 (s, H), 1.32

(s, 18H). MALDI-TOF MS *m/z*: 537, 560 $[M+Na]^+$, 576 $[M+K]^+$.

4.1.3. Synthesis of ZnP–Fc–C_{60}. A saturated methanol solution of $Zn(OAc)_2$ (5 ml) was added to a solution of **H_2P–Fc–C_{60}** (20 mg) in $CHCl_3$ (50 ml) and refluxed for 3 h. After cooling, the reaction mixture was washed with water twice and dried over anhydrous Na_2SO_4, and then the solvent was removed. Flash column chromatography on silical gel with $CHCl_3$ as the eluent gave **ZnP–Fc–C_{60}** as a dark solid (98% yield, 21 mg). ^{1}H NMR (400 MHz, $CDCl_3$): 9.12 (d, J=4.6 Hz, 2H), 9.03 (d, J=4.6 Hz, 2H), 8.89 (d, J=4.6 Hz, 2H), 8.81 (d, J=4.6 Hz, 2H), 7.74 (d, J=8.0 Hz, 2H), 7.61 (s, 2H), 7.51 (d, J=8.2 Hz, 2H), 7.35–7.31 (m, 6H), 5.25 (s, 1H), 5.21 (s, 1H), 5.17 (s, 2H), 4.81–4.75 (m, 1H), 4.73 (s, 2H), 4.66 (s, 2H), 4.24 (s, 3H), 4.16 (s, 6H), 4.10 (s, 6H), 3.91 (s, 12H), 3.82–3.73 (m, 1H), 3.18–3.05 (m, 1H), 2.45–2.31 (m, 1H), 1.79–1.67 (m, 2H), 1.39–1.22 (m, 18H), 0.89–0.84 (m, 3H). UV/vis (CH_2Cl_2) λ_{max} 431, 552, 592 nm; fluorescence (CH_2Cl_2) λ_{max} 596, 644 nm; FT-IR (KBr, cm^{-1}): 2923, 2851, 1736, 15797, 1498, 1456, 1406, 1349, 1270, 1238, 1196, 1164, 1126, 1104, 1003, 797, 722, 526. MALDI-TOF MS *m/z*: 2225.3 $[M+H]^+$, 1504.5 $[M+H^+]-720$, calcd=2223 ($C_{145}H_{85}N_5O_{13}FeZn$). Anal. Calcd for $C_{145}H_{85}N_5O_{13}FeZn$: C, 78.22; H, 3.85; N, 3.15. Found: C, 78.29; H, 3.89; N, 3.12.

ZnP–Fc: ^{1}H NMR (400 MHz, $CDCl_3$): 9.02 (s, 6H), 8.95 (d, J=4.6 Hz, 2H), 8.18 (d, J=8.2 Hz, 2H), 7.58 (d, J=8.2 Hz, 2H), 7.43–7.40 (m, 6H), 7.08–7.21 (m, 4H), 5.16 (s, 2H), 5.11 (s, 2H), 4.66 (t, J=1.5 Hz, 4H), 4.13 (s, 9H), 3.94 (s, 18H), 1.29 (s, 9H). UV/vis (CH_2Cl_2) λ_{max} 422, 548 nm, 588 nm; fluorescence (CH_2Cl_2) λ_{max} 596, 644 nm; FT-IR (KBr, cm^{-1}): 2933, 1733, 1579, 1495, 1456, 1406, 1348, 1271, 1236, 1201, 1169, 1125, 1001, 798, 723, 520. MALDI-TOF MS *m/z*: 1351 $[M+H]^+$, calcd=1350.3 ($C_{75}H_{66}N_4O_{13}$-FeZn). Anal. Calcd for $C_{75}H_{66}N_4O_{13}FeZn$: C, 66.60; H, 4.92; N, 4.14. Found: C, 66.63; H, 4.95; N, 4.13.

Acknowledgements

This work was supported by the National Natural Science Foundation of China (10474101, 50372070, 20531060, 20418001 and 20421101) and the National Basic Research 973 Program of China (2006CB300402). This project is partly supported by National Center for Nanoscience and Technology, China.

Supplementary data

Supplementary data associated with this article can be found, in the online version, at doi:10.1016/j.tet.2006.02.076. ^{1}H NMR spectra for **H_2P–Fc–C_{60}**, **H_2P–Fc**, **ZnP–Fc–C_{60}**, **ZnP–Fc**, **Fc–C_{60}** and H–H COSY spectra of **H_2P–Fc–C_{60}** are available.

References and notes

1. Gust, D.; Moore, T. A. *Science* **1989**, *244*, 35–41.
2. Wasielewski, M. R. *Chem. Rev.* **1992**, *92*, 435–461.
3. Paddon-Row, M. N. *Acc. Chem. Res.* **1994**, *27*, 18–25.
4. Bard, A. J.; Fox, M. A. *Acc. Chem. Res.* **1995**, *28*, 141–145.
5. Piotrowiak, P. *Chem. Soc. Rev.* **1999**, *28*, 143–150.
6. Gust, D.; Moore, T. A. In Kadish, K. M., Smith, K. M., Guilard, R., Eds.; The Porphyrin Handbook; Academic: San Diego, CA, 2000; Vol. 8, pp 153–190.
7. Imahori, H.; Yamada, K.; Hasegawa, M.; Taniguchi, S.; Okada, T.; Sakata, Y. *Angew. Chem., Int. Ed.* **1997**, *36*, 2626–2629.
8. Gust, D.; Moore, T. A.; Moore, A. L. *Acc. Chem. Res.* **2001**, *34*, 40–48.
9. Fukuzumi, S.; Imahori, H.; Yamada, H.; El-Khouly, M. E.; Fujitsuka, M.; Ito, O.; Guldi, D. M. *J. Am. Chem. Soc.* **2001**, *123*, 2571–2575.
10. Imahori, H.; Mori, Y.; Matano, Y. *Photochem. Photobiol., C* **2003**, *4*, 51–83.
11. Kanato, H.; Takimiya, K.; Otsubo, T.; Aso, Y.; Nakamura, T.; Araki, Y.; Ito, O. *J. Org. Chem.* **2004**, *69*, 7183–7189.
12. Imahori, H.; Hagiwara, K.; Aoki, M.; Akiyama, T.; Taniguchi, S.; Okada, T.; Shirakawa, M.; Sakata, Y. *J. Am. Chem. Soc.* **1996**, *118*, 11771–11782.
13. Armaroli, N.; Diederich, F.; Dietrich-Bucheeker, C. O.; Flamigni, L.; Marconi, G.; Nierengarten, J. F.; Sauvage, J. P. *Chem. Eur. J.* **1998**, *4*, 406–416.
14. Guldi, D. M. *Chem. Soc. Rev.* **2002**, *31*, 22–36.
15. Delgado, J. L.; de la Cruz, P.; López-Arza, V.; Langa, F.; Kimball, D. B.; Haley, M. M.; Araki, Y.; Ito, O. *J. Org. Chem.* **2004**, *69*, 2661–2668.
16. Fukuzumi, S.; Guldi, D. M. In *The Porphyrin Handbook*; Kadish, K. M., Smith, K. M., Guilard, R., Eds.; Academic: San Diego, CA, 2000; Chapter 8, pp 115–151.
17. Marcus, R. A. *Angew. Chem., Int. Ed. Engl.* **1993**, *32*, 1111–1121.
18. Marcus, R. A.; Sutin, N. *Biochim. Biophys. Acta* **1985**, *811*, 265–322.
19. Hayashi, T.; Ogoshi, H. *Chem. Soc. Rev.* **1997**, *26*, 355–364.
20. Solladie, N.; Walther, M. E.; Gross, M.; Duarte, T. M. F.; Bourgogne, C.; Nierengarten, J.-F. *Chem. Commun.* **2003**, 2412–2413.
21. Schuster, D. I.; Cheng, P.; Jarowski, P. D.; Guldi, D. M.; Luo, C. P.; Echegoyen, L.; Pyo, S.; Holzwarth, A. R.; Braslavsky, S. E.; Williams, R. M.; Klihm, G. *J. Am. Chem. Soc.* **2004**, *126*, 7257–7270.
22. Fujitsuka, M.; Ito, O.; Imahori, H.; Yamada, K.; Yamada, H.; Sakata, Y. *Chem. Lett.* **1999**, 721–722.
23. Imahori, H.; Tamaki, K.; Guldi, D. M.; Luo, C.; Fujitsuka, M.; Ito, O.; Sakata, Y.; Fukuzumi, S. *J. Am. Chem. Soc.* **2001**, *123*, 2607–2617.
24. Beer, P. D.; Drew, M. G.; Hesek, D.; Jagessar, R. *J. Chem. Soc., Chem. Commun.* **1995**, 1187–1189.
25. Beer, P. D.; Kurek, S. S. *J. Organomet. Chem.* **1987**, *336*, C17–C21.
26. Beer, P. D.; Kurek, S. S. *J. Organomet. Chem.* **1989**, *366*, C6–C8.
27. Wagner, R. W.; Brown, P. A.; Johnson, T. E.; Lindsey, J. S. *J. Chem. Soc., Chem. Commun.* **1991**, 1463–1466.
28. Burrell, A. K.; Campbell, W.; Officer, D. L. *Tetrahedron Lett.* **1997**, *38*, 1249–1252.
29. Schuster, D. I.; Cheng, P.; Wilson, S. R.; Prokhorenko, V.; Katterle, M.; Holzwarth, A. R.; Braslavsky, S. E.; Klihm, G.; Williams, R. M.; Luo, C.-P. *J. Am. Chem. Soc.* **1999**, *121*, 11599–11600.
30. Ajamaa, F.; Duarte, T. M. F.; Bourgogne, C.; Holler, M.; Fowler, P. W.; Nierengarten, J.-F. *Eur. J. Org. Chem.* **2005**, 3766–3774.

31. Eckert, J.-F.; Nicoud, J.-F.; Nierengarten, J.-F.; Liu, S.-G.; Echegoyen, L.; Barigelletti, F.; Armaroli, N.; Ouali, L.; Krasnikov, V.; Hadziioannou, G. *J. Am. Chem. Soc.* **2000**, *122*, 7467–7479.
32. de la Torre, M. D. L.; Marcorin, G. L.; Pirri, G.; Tomé, A. C.; Silva, A. M. S.; Cavaleiro, J. A. S. *Tetrahedron Lett.* **2002**, *43*, 1689–1691.
33. Suárez, M.; Verdecia, Y.; Illescas, B.; Martínez-Alvarez, R.; Alvarez, A.; Ochoa, E.; Seoane, C.; Kayali, N.; Martín, N. *Tetrahedron* **2003**, *59*, 9179–9186.
34. Olmstead, M. M.; Costa, D. A.; Maitra, K.; Noll, B. C.; Phillips, S. L.; van Calcar, P. M.; Balch, A. L. *J. Am. Chem. Soc.* **1999**, *121*, 7090–7097.
35. Boyd, P. D. W.; Hodgson, M. C.; Rickard, C. E. F.; Oliver, A. G.; Chaker, L.; Brothers, P. J.; Bolskar, R. D.; Tham, F. S.; Reed, C. A. *J. Am. Chem. Soc.* **1999**, *121*, 10487–10495.
36. Konarev, D. V.; Neretin, I. S.; Slovokhotov, Y. L.; Yudanova, E. I.; Drichko, N. V.; Shul'ga, Y. M.; Tarasov, B. P.; Gumanov, L. L.; Batsanov, A. S.; Howard, J. A. K.; Lyubovskaya, R. N. *Chem. Eur. J.* **2001**, *7*, 2605–2616.
37. Guldi, D. M.; Hirsch, A.; Scheloske, M.; Dietel, E.; Troisi, A.; Zerbetto, F.; Prato, M. *Chem. Eur. J.* **2003**, *9*, 4968–4979.
38. Souza, F. D.; Deviprasad, G. R.; Zandler, M. E.; El-Khouly, M. E.; Fujitsuka, M.; Ito, O. *J. Phys. Chem. B* **2002**, *106*, 4952–4962.
39. Armaroli, N.; Marconi, G.; Echegoyen, L.; Bourgeois, J.-P.; Diederich, F. *Chem. Eur. J.* **2000**, *6*, 1629–1645.
40. Sun, D.; Tham, F. S.; Reed, C. A.; Chaker, L.; Boyd, P. D. W. *J. Am. Chem. Soc.* **2002**, *124*, 6604–6612.
41. Lee, W. A.; Graetzel, M.; Kalyansundaram, K. *Chem. Phys. Lett.* **1984**, *107*, 308–313.
42. Knobloch, F. W.; Rauscher, W. H. *J. Polym. Sci.* **1961**, *54*, 651–656.
43. Xiao, S.-Q.; Li, Y.-L.; Li, Y.-J.; Yang, C.-H.; Liu, H.-B.; Ning, B.; Liu, Y.; Lu, F.-S.; Fan, L.-Z.; Zhuang, J.-P.; Li, Y.-F.; Zhu, D.-B. *J. Phys. Chem. B* **2004**, *108*, 16677–16685.